Ena/VASP-EVH1 inhibition prevents chemotaxis and metastasis by blocking the EVH1-WAVE2 interaction

Müller, M.; Barone, M.; Dinther, M. van; Motzny, K.; Ren, J.; Eichhorst, J.; ... ; Kühne, R.

PNAS RESEARCH ARTICLE | BIOCHEMISTRY CHEMISTRY OPEN ACCESS

Ena/VASP-EVH1 inhibition prevents chemotaxis and metastasis by blocking the EVH1–WAVE2 interaction

Matthias Müller[a,b,1,2], Matthias Barone[b,c,1], Maarten van Dinther[d], Kathrin Motzny[b], Jiang Ren[d], Jenny Eichhorst[b], Dominik Albat[a,e], Slim Chiha[a,e], Martin Lehmann[b], Rudolf Volkmer[b], Hartmut Oschkinat[b], Hans-Günther Schmalz[a,e], Peter ten Dijke[d,2], and Ronald Kühne[a,b,2]

Affiliations are included on p. 9.

Edited by Peter Devreotes, Johns Hopkins University School of Medicine, Baltimore, MD; received November 14, 2024; accepted May 23, 2025

Cancer therapy would benefit from suppressing cancer cell motility in the process of metastasis. Such directed cell migration relies on the propulsive force established by the filamentous actin network within lamellipodia. Proteins of the Ena/VASP family and the WAVE regulatory complex orchestrate lamellar protrusions and therefore provide promising targets for pharmacological interventions. Here, we report a cross-talk between Ena/VASP proteins and WAVE2 that is important for cancer cell extravasation. Mutating the EVH1 domain recognition motif in WAVE2 abrogates chemotaxis of triple-negative MDA-MB-231 breast cancer cells and reduces their extravasation in a zebrafish model. In pilot experiments, orthotopic implantation of these cells into mice led to a reduction in macrometastasis, resulting in prolonged survival. Similarly, intervention by an Ena/VASP-EVH1 inhibitor also reduced metastasis in vivo. Our results suggest that pharmacological interference with the Ena/VASP–WAVE2 interaction may thus reduce metastasis.

oncology | extravasation | metastasis | pharmacology | target validation

Significance

Protein–protein interactions mediated by proline-rich motifs (PRMs) play a crucial role in regulating important cellular signaling cascades associated with metastasis of malignant tumors and related death. Here, we show that the interaction between Ena/VASP and WAVE2 plays a role in orchestrating lamellipodial protrusions and cell movement. Disrupting this interaction shows promising results in inhibiting metastasis. The recognition motif within this interaction adopts a unique secondary structure that has been challenging to target with small molecules. However, we present a selective Ena/VASP-EVH1 inhibitor that is shown to target the Ena/VASP-WAVE2 interaction, besides others, showing the potential of developing pharmacological interventions that could effectively reduce metastasis and improve patient outcomes.

Metastasis is the defining hallmark of malignant tumors where directed cell migration, intravasation, and extravasation depend on gradients of chemoattractants such as specific chemokines and growth factors (1–3). Their receptors regulate cytoskeletal reorganization and motility (4) via activation of phosphoinositide 3-kinase (PI3K). In subsequent steps, Ras-associated and pleckstrin homology domain-containing protein 1 (RAPH1/lamellipodin) and the Wiskott–Aldrich syndrome verprolin-homologous (WAVE) proteins are recruited to the plasma membrane, triggering actin cytoskeleton remodeling (5–7) (Fig. 1*A*). WAVE proteins harbor a conserved C-terminal Verprolin-homology, Central, Acidic (VCA) sequence that stimulates the actin-nucleating and -branching activity of the actin-related protein 2/3 (ARP2/3) complex (8). In humans three WAVE paralogs, WAVE1, 2, and 3 have been described. While all three WAVE proteins connect polymerizing actin to the plasma membrane, paralog-specific properties likely arise due to differences in affinity for specific binding partners (9). An example is provided by guanosine triphosphate hydrolase (GTPase)-dependent localization of WAVE to the leading edge that is promoted by an interaction with the membrane-associated insulin receptor substrate p53 (IRSp53), where WAVE2 has a much higher affinity than WAVE1 or 3 (10). The WAVE proteins are members of the WAVE regulatory complex (WRC) (11, 12) in which Abelson interactor (ABI) links RAPH1 to WAVE (Fig. 1*A*). This interaction is relevant for regulating basal movements in cell migration (13). In addition, RAPH1 also binds to the three human paralogs: Enabled homolog (ENAH), Vasodilator-stimulated phosphoprotein (VASP), and Ena/VASP like (EVL). This interaction recruits Ena/VASP proteins to the leading edge of migrating cells (5, 6), a process which is essential for the chemotactic response to EGF in breast cancer metastasis (14).

Ena/VASP proteins consist of two Ena/VASP homology domains (EVH1 and EVH2) separated by a proline-rich central region. The EVH2 domains are associated with the actin filament barbed ends to accelerate polymerization, delay filament capping, and reduce ARP2/3-driven filament branching (15–20). The EHV1-domains recognize a short proline-rich consensus motif [D/E]–[F/W/L/Y]–Pxφ φP–[D/E] (21) (φ φ hydrophobic, x any amino acid) in poly-proline type II helix (PPII) conformation. This motif is presented by proteins located at sites of actin polymerization, particularly by ZYXIN in focal adhesions and by RAPH1 at the leading edge of migrating cells (22, 23). Ena/VASP proteins are involved in potentiating invasiveness (24), and their high expression is part of the invasive signature of many solid cancers such as breast cancer (25), colorectal cancer, pancreatic cancer, and gastric cancer (26–29).

Author contributions: M.M., H.-G.S., P.t.D., and R.K. designed research; M.M., M.B., M.v.D., K.M., and J.R. performed research; M.M., M.B., M.v.D., and J.R. analyzed data; J.E., D.A., S.C., M.L., R.V., and H.-G.S. contributed new reagents/analytic tools; and M.M., M.B., H.O., P.t.D., and R.K. wrote the paper.

Competing interest statement: P.t.D. is a scientific advisor for Prosion GmbH. S.C., H.-G.S., and R.K. hold shares of Prosion GmbH.

This article is a PNAS Direct Submission.

[1]M.M. and M.B. contributed equally to this work.

[2]To whom correspondence may be addressed. Email: Matthias.Mueller@prosion.eu, P.ten_Dijke@lumc.nl, or kuehne.ronald@gmx.de.

This article contains supporting information online at https://www.pnas.org/lookup/suppl/doi:10.1073/pnas.2423512122/-/DCSupplemental.

Published June 25, 2025.

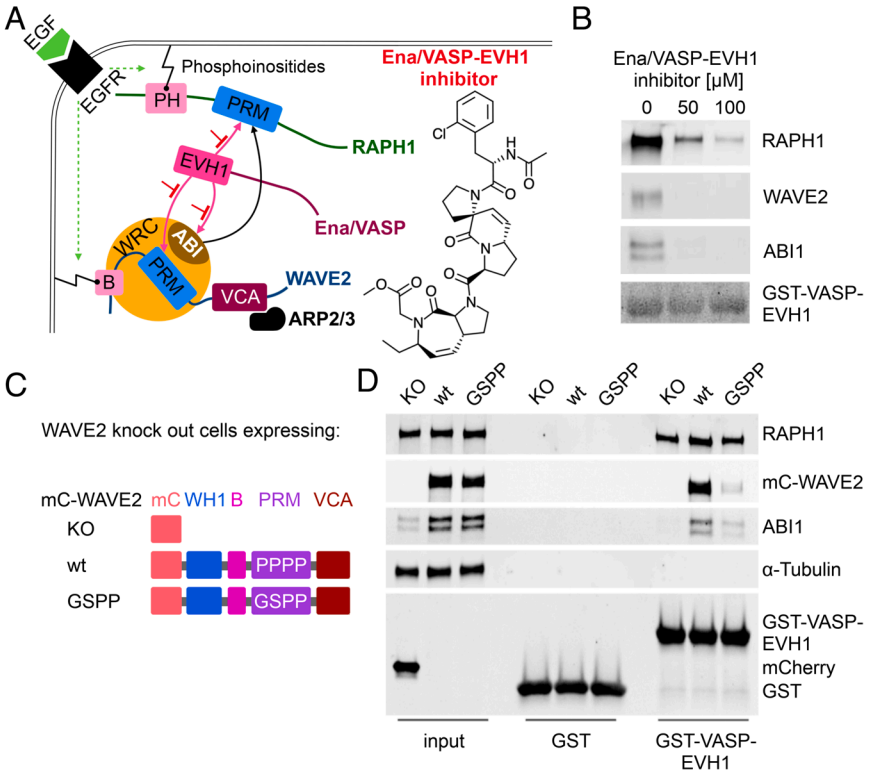

Fig. 1. WAVE2 binds with LPPPP motif to EVH1. (*A*) Schematic illustration of the Ena/VASP-EVH1 interactome at the leading edge. Epidermal growth factor receptor (EGFR) signaling leads to phosphoinositides-mediated membrane association of RAPH1 via the pleckstrin-homology (PH) domain and WAVE2 via the basic (B) region. The proline-rich motif (PRM) of RAPH1, and the WAVE regulatory complex (WRC) members WAVE2, and ABI interact with the Ena/VASP-EVH1 domain and interfere with the EVH1 inhibitor. WAVE2- verprolin homology/central/acidic (VCA) domain activates the ARP2/3 complex, enabling actin polymerization and leading-edge protrusion. (*B*) Pull-down assays with bead-immobilized GST-VASP-EVH1 using MDA-MB-231 cell lysate and Ena/VASP-EVH1 inhibitor. The Experiment was performed in two independent replicates. (*C*) WAVE2 constructs: WASP homology 1 domain (WH1), basic region (B), PRM, VCA, mCherry (mC), knockout (KO). (*D*) Pull-down assays with bead-immobilized GST-VASP-EVH1 or GST alone as a control using cell lysates from WAVE2^{KO}, mC-WAVE2^{wt}, or mC-WAVE2^{GSPP} cells. Input indicates equal expression rates for both WAVE2 constructs (panel mC-WAVE2, lanes 2 and 3) and mCherry (*Lower* panel, lane 1). Results were verified in two independent assays and representative results are shown.

In previous studies, we developed synthetic diproline mimetics called ProMs (30–36) and combined them to target Ena/VASP-EVH1 (37). These Ena/VASP-EVH1 inhibitors displaced VASP from the leading edge of triple-negative breast cancer (TNBC) cells, inhibited chemotaxis toward fetal bovine serum (FBS), and strongly reduced extravasation in a zebrafish xenograft model (37, 38). In this study, we use an optimized, membrane permeable derivative (Fig. 1*a*) with affinities around 400 nM toward each of the three Ena/VASP EVH1 domains (38).

Here, we report the identification of a recognition motif within WAVE2 enabling binding to the Ena/VASP-EVH1 domain and steering the Ena/VASP-driven cell chemotaxis. Experiments with genetically modified cells that do not contain the EVH1 binding motif in WAVE2 show changed lamellipodial protrusions, disturbed extravasation in zebrafish, and significantly reduced metastasis in mice. Similarly, we show that pharmacological inhibition of the Ena/VASP–WAVE2 interaction reduces metastasis in vivo.

Results

A PRM of WAVE2 Binds Directly to Ena/VASP-EVH1. Since our ProMs-based Ena/VASP-EVH1 inhibitor interferes with Ena/VASP interactions (Fig. 1*A*), it offers the opportunity to revisit the role of EVH1 domains in cancer cell migration. Therefore, we performed an interactome analysis by a pull-down assay employing immobilized, glutathione S-transferase (GST)-tagged VASP-EVH1 and MDA-MB-231 breast cancer cell lysate, in the presence or absence of the Ena/VASP-EVH1 inhibitor. The interaction partners that specifically bound to VASP-EVH1, were analyzed by tryptic digestion in ^{16}O and ^{18}O labeled water (with and without Ena/VASP-EVH1 inhibitor, respectively) and identified by their peptide pattern in reverse phase liquid chromatography tandem Mass-Spectrometry (RP-LC–MS/MS). Besides known interaction partners previously reported, including ZYXIN (39), RAPH1 (23), and ABI1 (40), we identified WRC member WAVE2, but not related members WAVE1 or WAVE3 (*SI Appendix*, Table S1), as interaction partner. Sequence comparison of all WRC proteins revealed that potential Ena/VASP-EVH1 binding motifs are only present in the PRM of WAVE2, which has been previously shown to interact with VASP in *Caenorhabditis elegans* (41).

Since WAVE2 is largely unstructured, we could not express it in soluble form. In such a case, it is a standard procedure to study the interaction of WAVE2-derived peptides with VASP-EVH1. Pepscan epitope mapping of WAVE2 binding to GST-VASP-EVH1 revealed a specific 15-mer WAVE2-derived peptide (*SI Appendix*, Fig. S1) that is conserved among different vertebrate species (*SI Appendix*, Table S2), but is absent in WAVE1 and WAVE3. This aligns with observations that EVH1 domains interact with a 12-residue sequence, including four prolines with an attached hydrophobic residue, flanked on both sides by acidic amino acids (21) (*SI Appendix*, Fig. S2). Binding was confirmed by isothermal titration calorimetry (ITC) measurements (K_d 250 μM) and revealed an affinity similar to one of the already known EVH1 binding motifs within RAPH1 (100 μM) (23) and ZYXIN (134 to 263 μM) (39).

In a pull-down assay with immobilized GST-VASP-EVH1 and MDA-MB-231 cell lysate we confirmed the ability of the Ena/VASP-EVH1 inhibitor to compete with both WRC

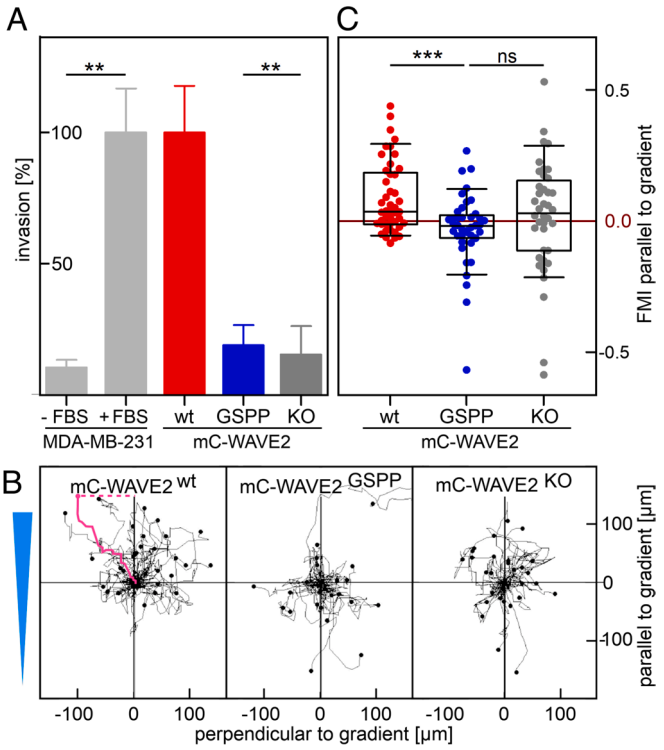

Fig. 2. EVH1–WAVE2 interaction is needed for chemotactic response of MDA-MB-231 cells. (*A*) Boyden chamber invasion assay with chemoattractant-containing FBS for MDA-MB-231 cells after 16 h incubation. MDA-MB-231 cells as a control with (+FBS) and without (−FBS). Mean ± SD normalized to MDA-MB-231 +FBS. Data from two independent experiments are shown. Statistical significance (**$P \le 0.01$) was evaluated using *t* test analysis. (*B*) Trajectories from live cell tracking of MDA-MB-231 cells. FBS gradient parallel to y-axis (light blue triangle). The forward migration index parallel to the gradient was calculated by normalizing the endpoint (magenta dashed line) by the accumulated distance (magenta solid line). (*C*) Forward migration index (FMI) from live cell tracking of MDA-MB-231 cells parallel to the gradient of chemoattractant-containing FBS. Only mC-WAVE2^{wt} shows a chemotactic response parallel to the FBS gradient, while mC-WAVE2^{KO} and mC-WAVE2^{GSPP} cells migrate randomly. Representative data from two independent experiments are shown. Statistical significance (***$P \le 0.001$, ns: not significant) was evaluated using the Mann–Whitney test.

members, WAVE2 and ABI1, as well as RAPH1 (Fig. 1*B*), which are part of the VASP interactome (13, 14, 40) (Fig. 1*A*). The inhibitor displaced all three proteins in a concentration-dependent manner. To conserve the function of the WAVE2 complex while abrogating the Ena/VASP-EVH1 interaction, we next sought for a minimal mutation within WAVE2. We, therefore, changed its EVH1 core motif amino acid sequence LPPPP to LGSPP. This is based on the observation that the 15-mer WAVE2-derived peptide Ac-SEDNLPPPPAEFSYP-NH_2, equipped with this substitution, dramatically lost affinity for VASP-EVH1.

To corroborate the specificity of the found motif, WAVE2 was knocked out in MDA-MB-231 cells by CRISPR/Cas9 using a sgRNA sequence homologous to the nucleotide sequence 221-240 of the *WAVE2* gene. Knockout was confirmed by western blot analysis (*SI Appendix*, Fig. S2). Subsequently, we reintroduced by lentiviral transduction mCherry-WAVE2 wild type (mC-WAVE2^{wt}) or a mCherry fusion construct harboring the core motif mutation LGSPP (mC-WAVE2^{GSPP}), or mCherry alone as a control (mC-WAVE2^{KO}, Fig. 1*C*). The level of expression is shown in *SI Appendix*, Fig. S2. We then repeated the pull-down assay with the lysates from these cell lines (Fig. 1*D*). The pull-down confirmed that WAVE2 harboring the nonfunctional recognition motif (mC-WAVE2^{GSPP}) showed impaired EVH1-mediated enrichment compared to mC-WAVE2^{wt}. Traces of mC-WAVE2^{GSPP} were observed, which potentially were mediated via the indirect interaction of VASP-EVH1 with ABI1, either as part of the WRC or with RAPH1. In line with a previous study (42), ABI1 expression was impaired in WAVE2 knockout cells (Fig. 1*D*, input). Reexpression of both WAVE2 variants (wt or GSPP amino acid motif) rescued ABI1 expression.

Disruption of the Ena/VASP–WAVE2 Interaction Is Crucial for MDA-MB-231 Cell Invasion, Impairs Chemotaxis, and Alters Lamellipodial Protrusions. WAVE2 stimulates nucleation and branching of actin in lamellipodia via ARP2/3, impacting cell migration. VASP has been shown to promote actin filament elongation and to reduce the density of ARP2/3-induced actin branching (16, 17). We, therefore, investigated the relevance of the Ena/VASP–WAVE2 interaction for migration of the triple-negative breast cancer cell line MDA-MB-231 in a Boyden chamber transwell invasion assay (Fig. 2*A*). As a control, MDA-MB-231 cells were tested with and without the chemoattractant-containing fetal bovine serum (FBS). The invasion was significantly enhanced toward FBS. MDA-MB-231 cells expressing mC-WAVE2^{KO} and mC-WAVE2^{GSPP} showed strongly reduced invasion comparable to control cells without FBS while mC-WAVE2^{wt} cells invaded comparable to the control with FBS. Impaired invasion of mC-WAVE2^{GSPP} cells was not a result of altered proliferation rates or weakened adhesion (*SI Appendix*, Fig. S3). We next investigated whether the reduced invasive potential of WAVE2^{GSPP} cells was due to reduced cell migration, the loss of chemotactic response, or the inability to stimulate the degradation of the extracellular matrix. The chemotactic response and the velocity of the cells expressing the WAVE2 variants were measured in a 2D live cell tracking assay employing a gradient of chemoattractant-containing FBS. From the trajectories of the cells (Fig. 2*B*) the forward migration index (FMI) for every individual cell was calculated parallel to the gradient by normalizing the endpoint to the accumulated distance (Fig. 2*B*, magenta lines). The velocity was calculated by dividing the accumulated distance by the cell migration time (*SI Appendix*, Fig. S4). A chemotactic response is given when the tail of distribution of the cellular FMIs is larger than zero (Fig. 2 *C*, *First* lane). If the tailing is oriented to both sides, in positive and negative directions, migration is termed random (Fig. 2 *C*, *Second* lane). In line with a previous study (18), mC-WAVE2^{KO} cells migrated randomly and with reduced velocity. Only mC-WAVE2^{wt} cells showed a chemotactic response. However, mC-WAVE2^{GSPP} cells migrated randomly but at the same speed as mC-WAVE2^{wt} cells.

FBS contains a mixture of different growth factors and chemokines. To test chemotaxis with a more specific chemoattractant, we verified the ability of MDA-MB-231 cells to follow a gradient of epidermal growth factor (EGF) (*SI Appendix*, Fig. S5), as it is known that EGF promotes invasion through RAPH1 interaction with WAVE and Ena/VASP, and promotes metastasis formation in vivo (13, 14).

Since cells lacking the EVH1 binding motif in WAVE2 exhibited impaired chemotaxis, we checked whether mC-WAVE2^{wt} and mC-WAVE2^{GSPP} cells might show different lamellipodial protrusions at the leading edge (LE). For this purpose, filamentous actin (F-actin) was visualized in cells expressing near-infrared fluorescent protein (iRFP)-lifeAct using total internal reflection fluorescence (TIRF) microscopy. Upon EGF stimulation, the velocity of membrane protrusions was examined using kymographs (*SI Appendix*, Fig. S6), analyzing the growing LE and faster membrane protrusions, referred to here as membrane bursts, that occurred in a pulsating manner (Fig. 3 *A*, *Left* panel). Both the protrusion of the LE and membrane bursts at the LE were

significantly slower for mC-WAVE2^{GSPP} cells than mC-WAVE2^{wt} cells (Fig. 3 *A*, *Right* panel).

Studying the recruitment of VASP to the leading edge upon EGF stimulation in immunofluorescence stains (Fig. 3*B*), we found that the mutant mC-WAVE2^{GSPP} cells showed reduced VASP accumulation to the LE compared to the wild type (Fig. 3 *C*, *Right* panel). The amount of F-actin within the lamellipodia was also reduced in mC-WAVE2^{GSPP} cells (Fig. 3 *C*, *Left* panel). This correlates with the results from the lamellipodial protrusion velocity (Fig. 3*A*). We conclude that the Ena/VASP-EVH1–WAVE2 interaction enhances Ena/VASP corecruitment to the LE driving both the lamellipodial protrusion velocity and the formation of spatiotemporal membrane bursts by enhancing F-actin synthesis, in this way enabling a chemotactic response.

We next investigated whether actin polymerization was altered when the Ena/VASP–WAVE2 interaction was impaired. We recombinantly expressed short VCA- SEDNLPPPPAEFSYP fusion (PRM^{wt}-VCA) constructs that comprised the 15-amino acid binding site, but not the other residues of the proline-rich region of WAVE2 (Fig. 3*D*). A construct with the corrupted binding site (GSPP, PRM^{GSPP}-VCA) was also made. With both, we performed in vitro actin polymerization assays. Adding the two constructs to ARP2/3 and profilin induced equal actin polymerization signals (Fig. 3*D*, orange and light blue curves). Combining PRM^{wt}-VCA with VASP (Fig. 3*D*, red curve), significantly boosted F-actin synthesis rates. In contrast, when PRM^{GSPP}-VCA was combined with VASP (Fig. 3*D*, blue curve) actin polymerization rates remained unchanged, suggesting that the interaction of WAVE2 with the VASP-EVH1 domain is important to increase VASP-dependent actin polymerization velocity, directing lamellipodial protrusions and thereby enabling improved chemotaxis.

Disruption of the Ena/VASP–WAVE2 Interaction Causes a Lower Rate of MDA-MB-231 Cell Metastasis and Prolongs Survival In Vivo. To estimate the potential of the described interaction as a target for drugs reducing metastasis, we employed zebrafish and mouse xenograft models with MDA-MB-231 cells exhibiting a corrupted Ena/VASP-EVH1 binding site in their WAVE2 proteins.

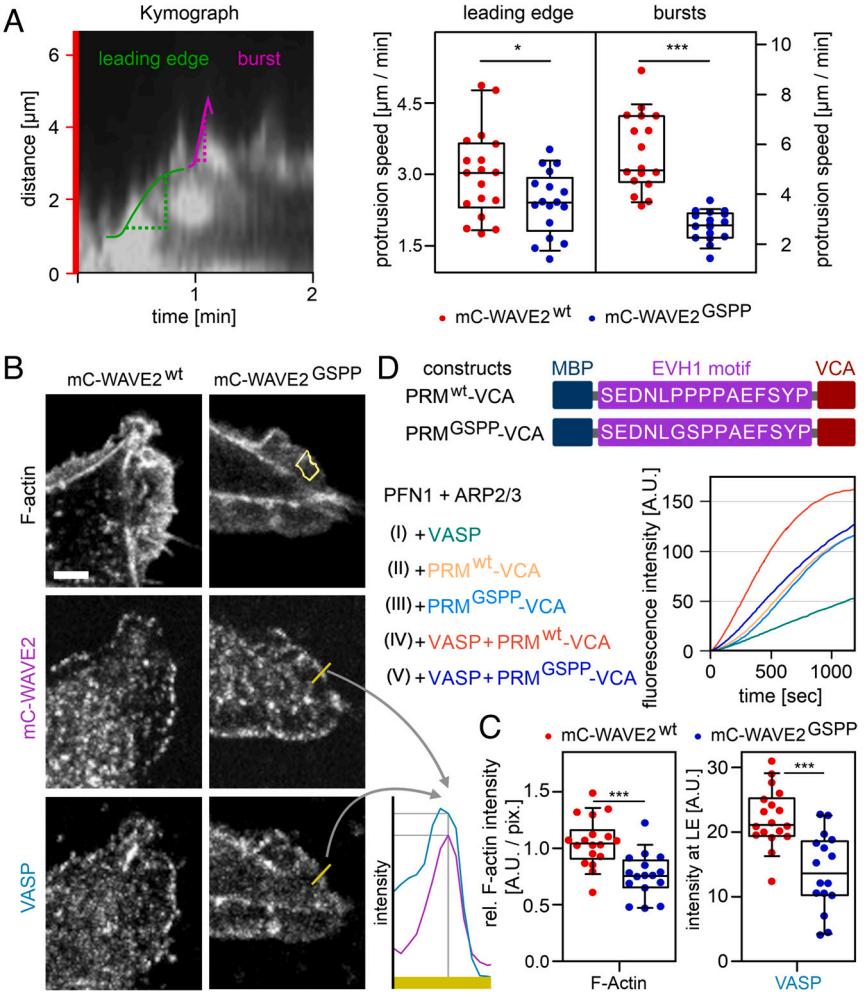

Fig. 3. EVH1–WAVE2 interaction modulates actin polymerization rates and lamellipodial protrusion velocity. (*A*) Lamellipodial protrusions. *Left* panel: A kymograph of membrane protrusions upon stimulation with EGF after starvation in MDA-MB-231 cells with time on the x-Axis and lamellipodial protrusion along a red bar (*SI Appendix*, Fig. S6) from TIRF micrographs. The protrusion velocity of the leading edge (green) and fast membrane burst protrusion (pink) were calculated. *Right* panel: Statistical evaluation of protrusion speeds for mC-WAVE2^{wt} and mC-WAVE2^{GSPP} cells. Data from three independent experiments are shown. *T* test analysis for leading edge (*$P \le 0.05$) and Mann-Whitney test for the bursts (***$P \le 0.001$). (*B*) Immunofluorescence stains (confocal micrographs) for F-actin, mCherry-WAVE2 constructs, and VASP in MDA-MB-231 cells stimulated with EGF after starvation and the statistical evaluation (*C*). Lamellipodia were identified via F-actin stain, and signal intensity was measured (the yellow area in the *Upper Right* panel represents the measured region of interest). The profile of WAVE2 and VASP (yellow bar in *Middle* and *Lower Right* panels) was plotted (*Lower Right* panel) and the intensities for both proteins were measured at maximal WAVE2 signal, indicating the leading edge. The scale bar (white) represents 5 µm. (*C*) Statistical evaluation of immunofluorescence stains. The F-actin intensity in the lamellipodia (*Left* panel) and VASP (*Right* panel) in the leading edge was evaluated. Data from two independent experiments. *T* test analysis (***$P \le 0.001$)). (*D*) In vitro actin polymerization assay of pyrene-labeled G-actin in the presence of profilin (PFN1) and ARP2/3 complex. WAVE2 constructs: maltose binding protein (MBP); WAVE2 motif recognized by EVH1 (wt) and the nonbinding mutant (GSPP); VCA domain. Raw fluorescence signal over time.

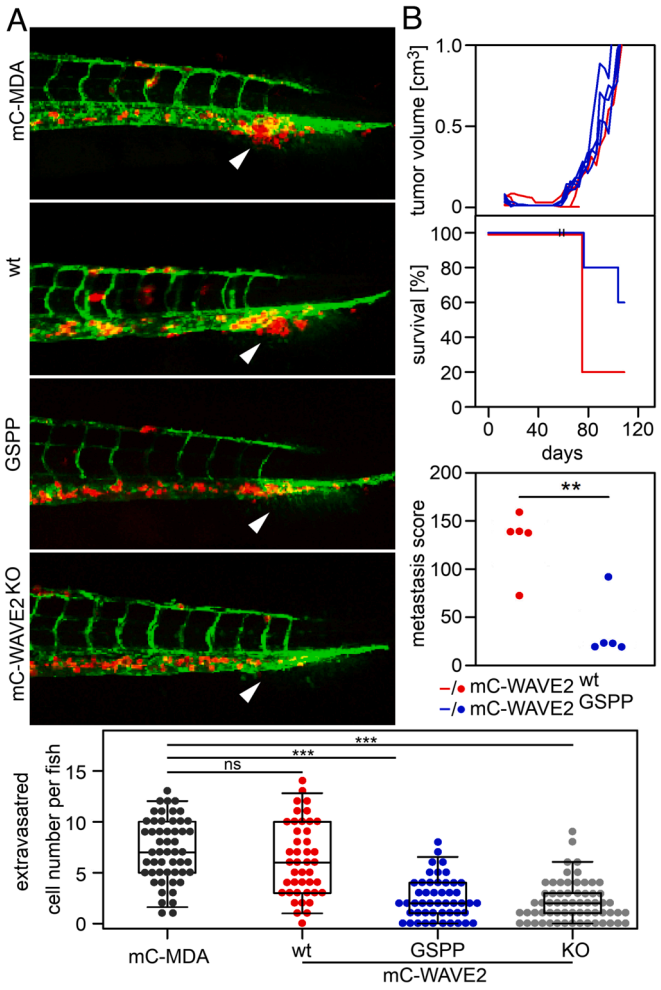

Fig. 4. EVH1–WAVE2 interaction enables MDA-MB-231 cell extravasation and metastasis in vivo. (*A*) Extravasation into the avascular collagen matrix-rich tailfin of zebrafish. Upper panel: micrographs of transgenic zebrafish. Vasculature (green) and mCherry expressing MDA-MB-231 cancer cells (red). White arrows indicate the region of extravasation. Lower panel: statistical evaluation of extravasated cancer cells per fish. Data from three independent experiments, and representative results are shown. Statistical significance (ns: not significant, ***$P \leq 0.001$) was evaluated using *t* test analysis. (*B*) Xenograft mouse experiment with MDA-MB-231 cells. NOG mice with orthotopically implanted mC-WAVE2^{wt} (red) and mC-WAVE2^{GSPP} (blue) cells. Upper panel: primary tumor volume over time. Middle panel: survival (red and blue lines) with two dropouts per group at day 53 (II). These animals were killed to ensure metastasis development. Lower panel: Metastasis score (red and blue dots). Metastasis score was determined ex vivo after the termination of each animal and represents the sum of all found metastasis in mm^2 visible on the surface of the liver and lung measured with a caliper. Statistical significance (**$P \leq 0.01$) was evaluated using *t* test analysis.

To investigate the effect of this modification on extravasation, we injected MDA-MB-231 breast cancer cells either expressing mC-WAVE2^{KO}, mC-WAVE2^{wt}, mC-WAVE2^{GSPP}, or solely mCherry (mC-MDA) into the embryonic circulation of transgenic *fli: enhanced green fluorescent protein* (EGFP) zebrafish (43); *fli:*GFP labels the vasculature green. The ability of these cells to extravasate into the avascular collagen matrix-rich tailfin (44) was determined by fluorescence microscopy and manual cell counting. The control mC-MDA cells and mC-WAVE2^{wt} cells equally invaded the avascular tailfin, while extravasation of mC-WAVE2^{KO} and mC-WAVE2^{GSPP} cells was significantly reduced (Fig. 4*A*). These results match the effects seen in the in vitro invasion assay (Fig. 2*A*). It is further in line with our earlier observation that the Ena/VASP-EVH1 inhibitor used here was able to prevent MDA-MB-231 tailfin invasion in the same zebrafish xenograft model (38).

Next, we investigated the effect of an impaired Ena/VASP–WAVE2 interaction in an orthotopic xenograft mouse experiment. To this end, female nude mice were orthotopically xenografted with the MDA-MB-231 cells either expressing mC-WAVE2^{wt}, or mC-WAVE2^{GSPP}.Cancer development was allowed to progress until mice reached the ethical termination criteria. In all mice, primary tumor growth was comparable (Fig. 4 *B*, *Upper* panel), which aligns with our finding that the introduced WAVE2 modification does not impact the proliferation or survival of cancer cells (*SI Appendix*, Fig. S3) overall. In contrast, the survival of mice with mC-WAVE2^{GSPP} cells implanted was enhanced, whereas mice with implanted mC-WAVE2^{wt} cells were much earlier moribund (Fig. 4 *B*, *Middle* panel). Once mice were terminated from the study, macrometastases were quantified. Mice with MDA-MB-231 cells expressing mC-WAVE2^{GSPP} showed a significantly reduced number of metastases compared to animals injected with mC-WAVE2^{wt} expressing cells (Fig. 4 *B*, *Lower* panel), further supporting the importance of the Ena/VASP–WAVE2 interaction for driving MDA-MB-231 cell metastasis formation *in vivo.*

The Ena/VASP-EVH1 Inhibitor Reduces Metastasis of PANC-1 Pancreatic Cancer Cells. Having shown that the interaction of the Ena/VASP-EVH1 domain with WAVE2 is relevant for actin polymerization velocity, chemotaxis, extravasation, and MDA-MB-231 breast cancer metastasis in vivo, we next investigated the effect of the Ena/VASP-EVH1 inhibitor on other cancer types. We decided to study pancreatic cancer, one of the most aggressive tumor types rapidly forming metastases (45, 46).

As a prerequisite, we performed a pharmacokinetic study comparing compound concentrations in the blood plasma after a single subcutaneous (s.c.) administration of 100 mg/kg with the compound release by an osmotic pump that corresponds to an application of 200 mg/kg per day (Fig. 5*a*). Application via the osmotic pump could maintain a plasma concentration of 1 µM 48 h post-transplantation, whereas the s.c. route led to 8 µM peak concentration with rapid decrease, resulting in concentrations as low as 1.6 nM within 6 h and of a value below the detection limit (1nM) after 24 h. Both routes have the same area under the curve (AUC), but s.c. application shows a much higher maximal plasma concentration (C_{max}). An s.c. approach with 100 mg/kg twice a day could boost the AUC by a factor of two. Therefore, the s.c. route is preferable as both AUC and C_{max} have higher values.

To evaluate the efficacy of the Ena/VASP-EVH1 inhibitor on pancreatic cancer, PANC-1 cells were orthotopically transplanted into female nude mice. The animals were treated with s.c. injections of 100 mg/kg Ena/VASP-EVH1 inhibitor twice daily from the day after tumor transplantation. We applied our inhibitor to mice, considering EVH1 domains are surprisingly conserved between *Homo sapiens* and *Mus musculus*. In fact, the ENAH-EVH1 domains are identical and the VASP-EVH1 domains differ in only 6 amino acids that are not part of the binding groove. However, no impact on body weight was observed, suggesting that the inhibitor concentration was well tolerated (Fig. 5*B*). At the end of a treatment period of 48 d, the Ena/VASP-EVH1-inhibitor treated group showed reduced macrometastasis while the primary tumor size was unchanged (*SI Appendix*, Fig. S7). This reduction was statistically significant (Fig. 5*C*). Regarding the weights of the liver and lung, a statistical lower weight could be observed only for the liver of EVH1 inhibitor-treated mice and might be an indicator for a lower metastatic burden. These results further support the

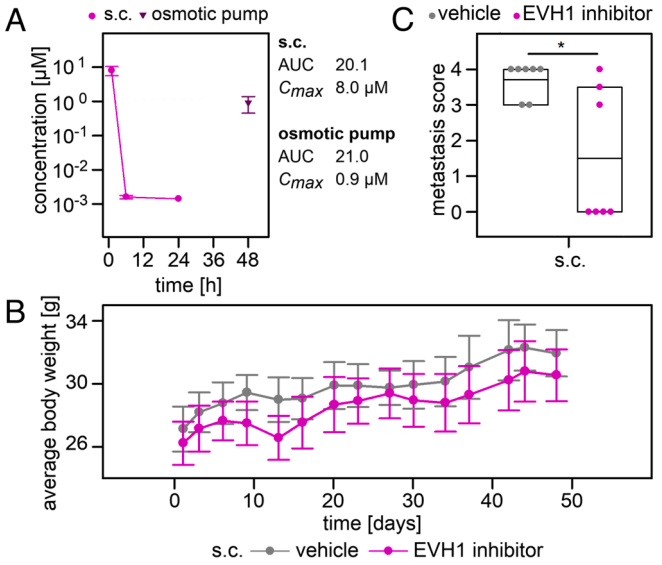

Fig. 5. The Ena/VASP-EVH1 inhibitor reduces PANC-1 cell metastasis in vivo. (*A*) Mouse pharmacokinetics of the Ena/VASP-EVH1 inhibitor comparing subcutaneous (s.c) injection (dots) with the implantation of an osmotic pump (triangle). Analysis was performed in triplicates, and plasma concentrations are given as mean ± SD. Area under the curve (AUC) and maximal plasma concentration (*Cmax*) were calculated. (*B*) Average animal body weight of xenograft mouse experiment. Ena/VASP-EVH1 inhibitor (pink) and vehicle (gray) treated animals with s.c. application. (*C*) Metastasis scores of xenograft mouse experiment with orthotopically implanted PANC-1 cells. Animals were treated with the Ena/VASP-EVH1 inhibitor (pink) or vehicle (gray) with s.c. application. Metastasis score was determined ex vivo after the termination of all animals and represents the sum of all found metastasis in mm^2 visible on the surface of the liver, lung, and spleen. Statistical significance (*$P \leq 0.05$) was evaluated using the Mann–Whitney test.

potential of Ena/VASP-EVH1 inhibitors as therapeutics for cancer metastasis prevention.

Discussion

Ena/VASP family proteins regulate cell actin dynamics, enabling chemotaxis, migration, and invasion. Ena/VASP upregulation has been described for many types of cancer, such as breast cancer, colorectal cancer, pancreatic cancer, and gastric cancer (25–29), rendering Ena/VASP proteins as promising therapeutic targets. In earlier studies, we described a selective Ena/VASP-EVH1 inhibitor that blocks invasion and extravasation of MDA-MB-231 breast cancer cells (37, 38). In this study, we shed further light on the molecular mechanisms exploited by the Ena/VASP-EVH1 inhibitor. Based on an interactome analysis, we identified an EVH1 recognition motif within WAVE2 that interacts with Ena/VASP-EVH1 domains. With a WAVE2 knockout clone overexpressing a functional (mC-WAVE2^{wt}) or EVH1-binding deficient (mC-WAVE2^{GSPP}) variant of WAVE2, we report the relevance in regulating protrusion velocities at the leading edge of migrating cells, impacting chemotaxis and as such contributing to the formation of MDA-MB-231 cell metastasis in vivo. The phenotypic rescue of mC-WAVE2^{wt} cells was confirmed in two independent assays. There is no difference between mC-WAVE2^{wt} and MDA-MB-231 cells in the invasion assay (Fig. 2*A*), nor in the extravasation into the collagen fibers of the tail fin in the zebrafish experiments (Fig. 4*A*).

In the context of WAVE1-containing WRC, Ena/VASP-EVH1 - WRC interaction via ABI1 increases cell migration and enables VASP to cooperatively enhance WRC stimulation cooperatively (40). Our pull-down assay shows that GST-VASP-EVH1 can only enrich ABI1 from lysates with impaired Ena/VASP-EVH1–WAVE2 interaction to a much lower extent compared to lysates with an intact interaction (Fig. 1*D*, columns 8 and 9). Here, ABI1 binds directly Ena/VASP-EVH1 (40) or via RAPH1 (13), which in turn binds itself effectively to Ena/VASP-EVH1. It appears that WAVE2 enhances ABI1 enrichment on beads presenting GST-VASP-EVH1. These results indicate that Ena/VASP-EVH1 binding to WAVE2 further increases affinity between Ena/VASP and the WRC, likely stabilizing the multiprotein complex. Among the three WAVE paralogs only WAVE2 exhibits the found EVH1 binding motif (*SI Appendix*, Table S3). These findings indicate that the WRC containing WAVE2 has a higher affinity to Ena/VASP. This increase of binding strength represents a difference between WAVE2 and the other two WAVE paralogs. Furthermore, among the three WAVE paralogs WAVE2 is the highest expressed member in invasive breast cancer (47).

Our results show that the WAVE2 interaction with Ena/VASP-EVH1 impacts extravasation (Fig. 4*A*). In a previous study, we showed that Ena/VASP enrichment at the leading edge of migrating cells relies on the activity of their EVH1 domain since the Ena/VASP-EVH1 inhibitor displaced VASP from that region (37). In a tripartite complex, RAPH1 binds to both the Ena/VASP proteins for recruiting them to the leading edge, and ABI as part of the WRC (23, 48) The interaction of Raph1 with the WRC, but not with Ena/VASP is required for random cell migration (13). Different mechanisms are involved in the directed migration of cells. Chemotaxis of cells toward EGF initiates RAPH1-dependent recruitment of Ena/VASP to the leading edge and promotes intravasation, but not extravasation (14). Here, we show that the Ena/VASP–WAVE2 interaction is key in extravasation (Fig. 4*A*). Furthermore, the abrogation of the interaction leads to a reduced amount of VASP in the leading edge, indicating that not only RAPH1 but also WAVE2 recruits Ena/VASP independently.

The WRC containing WAVE and ABI1 is the main activator of the ARP2/3 complex for actin filament nucleation and assembly in the lamellipodia of moving cells. In an in vitro actin polymerization assay, PRM^{wt}-VCA initiates faster actin polymerization than PRM^{GSPP}-VCA in combination with VASP (Fig. 3*D*). Ena/VASP proteins associate to actin filaments via their F-actin binding (FAB) and G-actin binding (GAB) sites (49). VASP only binds to and elongates barbed ends when its GAB associates with monomeric actin, otherwise it binds to actin filaments offsite the barbed ends via FAB (50). Therefore, the WRC may increase the number of Ena/VASP proteins associated with barbed ends, resulting in increased polymerization rates. In the context of our study, the increased actin polymerization rate of the PRM^{wt}-VCA–VASP complex might explain the different velocities of membrane protrusions seen in the TIRF kymographs (Fig. 3*A*) and might contribute to the observed effects on chemotaxis and extravasation.

Data from our orthotopic mouse model showed that impaired chemotaxis and extravasation properties of mC-WAVE2^{GSPP} are in line with a strongly reduced metastatic burden, while the primary tumor size is consistent with that of mC-WAVE2^{wt}. This is a major step in validating Ena/VASP-EVH1 as a relevant cancer metastasis target. To what extent the reduction of metastatic burden can be achieved as well by effective Ena/VASP-EVH1 inhibitors was examined in a proof of concept in vivo study. We started with investigation of the pharmacokinetic properties of the EVH1 inhibitor comparing subcutaneous injection (s.c.) with application via an osmotic pump (Fig. 5*A*). We aimed an inhibitor plasma concentration of at least 1 µM as this concentration reduced extravasation of MDA-MB-231 cancer cells in transgenic zebrafish significantly (38). Application via the osmotic pump maintained the 1 µM whereas the s.c. route led to an almost 10 times higher C_{max}, but with rapid decrease. Although both routes showed a similar area under the curve, with an application twice daily, the

s.c. route has the advantage of having an AUC that could double the one from the osmotic pump. Furthermore, a longer treatment time is possible as osmotic pumps are restricted to a duration of 28 d.

Employing an orthotopic PANC1 pancreatic cancer model with s.c. application twice a day, we indeed observed a reduction of macrometastasis (Fig. 5*C*). In fact, four out of seven inhibitor-treated mice did not show metastases at all in our experiment, whereas all untreated mice did.

Taken together, the results are consistent with the notion that the Ena-VASP-EVH1 inhibitor targets all EVH1 interactions of the Ena/VASP family. The WAVE2 - Ena/VASP-EVH1 domain interaction is one of many that are subject to interference. However, our experiments demonstrate the importance of the Ena/VASP family–WAVE2 interactions.

In conclusion, our data strongly demonstrate the impact of the Ena/VASP–WAVE2 interaction on actin-dependent motility through its involvement in lamellar protrusions, invasion, and extravasation. Moreover, our data indicate that metastasis, a more complex process involving additional factors, could be affected, and disrupting the interaction could be an avenue to a viable therapeutic strategy. Therefore, the improvement of pharmacological properties of the inhibitor and larger-scale studies with additional transgenic or syngenic cancer models are needed to finally clarify how strongly the metastasis of solid tumors can be influenced and are the subject of future investigations.

Materials and Methods

Plasmid Production and Protein Purification. Plasmid coding for Glutathione-(S)-Transferase (GST)-fused human VASP-EVH1 (human vasodilator-stimulated phosphoprotein, aa1–115) was provided by Dr. Linda Ball (FMP, Berlin, Germany) (51). Full-length VASP was cloned into pET28a (Novagen) and human Profilin into pGEX-4T-1 (Clontech) from a cDNA library (Clontech). WAVE2 was cloned from human cDNA (MGC human WASF2 cDNA, Thermo Fisher scientific) into pLV-mCherry [pLV-mCherry was a gift from Pantelis Tsoulfas (Addgene plasmid # 36084; http://n2t.net/addgene:36084; RRID:Addgene_36084)] and VCA constructs were cloned into pMal-c2X [pMAL-c2X was a gift from Paul Riggs (Addgene plasmid # 75286; http://n2t.net/addgene:75286; RRID:Addgene_75286)]. Mutants were prepared via site-directed mutagenesis by overlap extension PCR using mutagenic primers. For CRISPR/Cas9 knockout, the WAVE2 nucleotide sequence 221-240 (NM_006990.5, NCBI) was cloned into gRNA in pX330-U6-Chimeric_BB-CBh-hSpCas9 as described before (52). pX330-U6-Chimeric_BB-CBh-hSpCas9 was a gift from Feng Zhang (Addgene plasmid # 42230; http://n2t.net/addgene:42230; RRID:Addgene_42230).

Proteins were expressed in *E. coli* BL21(DE3) and grown in 2YT medium overnight. After sonification and centrifugation, the soluble fraction was purified according to the tag. GST-VASP-EVH1 and GST-PFN1 were loaded on a glutathione sepharose matrix, eluted with glutathione, and GST was cleaved overnight with thrombin. His-tagged full-length VASP was loaded to a Ni-NTA matrix and eluted with imidazole. Maltose binding protein (MBP)-tagged fusion constructs of the EVH1 binding motif within the PRM and the verprolin homology/central/acidic (VCA) domain of WAVE2 (MBP-PRM-VCA) were loaded to a MBP Trap HP column (GE), eluted with maltose and further purified as described before (53). Proteins were rebuffered by passing over a HiLoad 16/60 Superdex 75 or 200 size exclusion column (GE) and purity was verified via sodium dodecyl sulfate - polyacrylamide gel electrophoresis (SDS-PAGE).

Pull-Down Assay and Western Blot. Pull-down experiments were performed with GST-tagged VASP-EVH1 immobilized on glutathione Sepharose 4B beads (GE) using lysates from MDA-MB-231 or indicated cell lines derivatives thereof with a total protein concentration of 2 mg/ml, measured via BCA Protein Assay Kit (Pierce) and ultraviolet/visible (UV/VIS) spectroscopy (NanoDrop 1000; Thermo Fisher Scientific). Displacement of binding partners was performed by adding different concentrations of the Ena/VASP-EVH1 inhibitor to the lysate, incubating overnight on beads at 7 °C. GST alone was immobilized as a control to the beads and treated with lysate. Eluates were used for either $^{16}O/^{18}O$ -labeling followed by quantitative mass spectrometry or western blot analysis. The western blot with target-specific antibodies against RAPH1 [rabbit anti-RAPH1 (1:1,000); scbt], WAVE2 [rabbit anti-WAVE2 (1:1,000); Cell Signaling], ABI1 (rabbit anti-ABI1 (1:1,000); Cell Signaling], GST [rabbit anti-GST (1:1,000); scbt], mCherry [rabbit anti-mCherry (1:1,000); Invitrogen], Glyceraldehyde 3-phosphate dehydrogenase (GAPDH) [mouse anti-GAPDH (1:1,000); SCBT], and α-Tubulin [mouse anti-α-Tubulin (1:1,000); Cell Signaling] and fluorescence of secondary antibody (IRDye 800; Licor) was measured on an infrared scanner (ODYSSEY; Li-Cor, v2.0.40).

$^{16}O/^{18}O$-Labeling and Quantitative Mass Spectrometry. Eluates from GST-VASP-EVH1 bound beads incubated with MDA-MB-231 cell lysate in the presence or absence of 100 μM EVH1 inhibitor were separated by SDS-PAGE side-by-side. Tryptic in gel digest, $^{16}O/^{18}O$ labeling, nano-LC-mass spectrometry analysis, and data processing and quantification were performed as described before (54).

Pepscan Assay. An automated spot synthesis protocol on whatman-50-cellulose was used to prepare SPOT array (55). WAVE2 peptide sequence was spotted in 15-mer peptides with an overlap of 2 amino acids. Membranes with bound peptides were washed with ethanol and washing buffer [0.1% (v/v) tween-20, 1× TBS pH 8.6] and subsequently blocked with blocking buffer [1× TBS with 5% (w/v) milk powder, 0.1% (v/v) tween-20, pH 8.6] for 60 min at room temperature. The membranes were covered with GST-VASP-EVH1 or GST alone as a control (10 μg/ml) in sample buffer [1× TBS with 3% (w/v) milk powder, 0.1% (v/v) tween-20, pH 8.6] and incubated at 7 °C overnight. After extensive washing, the far-western blot with target-specific antibodies against GST [rabbit anti-GST (1:1,000); scbt], and the fluorescence of secondary antibody (IRDye 800; Licor) was measured on an infrared scanner (ODYSSEY; Li-Cor, v2.0.40).

Binding Studies. Dissociation constants were determined via ITC (37) (MicroCal, Malvern). All experiments were performed at 25 °C in 40 mM sodium phosphate, 100 mM sodium chloride, 2 mM TCEP, pH 7.3, and dissociation constants were calculated with peaq-itc analysis software.

Cell Culture. MDA-MB-231 (ATCC HTB-26) cells were cultured in RPMI with 10% FBS at 37 °C and 5% CO_2 atmosphere. Cells were regularly tested for the absence of *Mycoplasma*, and the authenticity was tested by SNP analysis (Eurofins Genomics).

CRISPR/Cas9 Knockout of WAVE2 and Restorage by wt or mt mCherry-WAVE2. MDA-MB-231 cells were transfected with pX330-U6-Chimeric_BB-CBh-hSpCas9 containing a gRNA sequence homologous to WAVE2 via Lipofectamine LTX with Plus reagent (Thermo Fisher Scientific) according to the manufacturer's instructions and subcultivated as single cell in 96-well plates. Clones were tested for WAVE2 expression in western blot with target-specific antibody to identify a knockout clone.

To restore WAVE2, either mCherry-WAVE2 wt or mCherry-WAVE2 mt, and as a control, mCherry alone was lentivirally transduced using pLV-mCherry constructs.

Immunofluorescence Staining. MDA-MB-231 derived cells were seeded into starvation medium (RPMI containing 1% bovine serum albumin (BSA), 0.05% FBS) in 8-well μ-slides (ibidi) coated with fibronectin (Roche). After 24 h, cells were stimulated with 500 ng/ml EGF (cell signaling) in RPMI for 1 min, followed by fixation with 4% p-formaldehyde and permeabilization with 0.1% Triton-X 100. For target-specific immunofluorescence staining, the cells were blocked with fish skin gelatin (Sigma), incubated with specific primary antibodies [rabbit anti-WAVE2 (1:50), cell signaling; mouse anti-VASP (1:1,000), ImmunoGlobe] followed by the corresponding secondary antibodies [anti-rabbit IgG Fab2 Alexa 647 (1:1,000), cell signaling; anti-mouse IgG Fab2 Alexa 488 (1:1,000), cell signaling], and Alexa 405 Phalloidin (Thermo) to stain for F-actin. Micrographs were taken on a confocal microscope (LSM 710, Zeiss) and evaluated using ImageJ (imagej.nih.gov/ij/; NIH).

Cell Invasion Assay. The BD Matrigel invasion chamber 24-well cell-invasion assay (BD Biosciences, Inc.) with 8 μm pore size was performed as described in the manufacturer's instructions. The experiments were done in triplicate with 50,000 cells (MDA-MB-231 or indicated cell lines derivatives thereof) per well in i) FBS gradient [10/0% (vol/vol)] and ii) FBS without a gradient (10% (vol/vol)). After 16

h of incubation, cells were fixed with 4% p-formaldehyde and stained with crystal violet. Micrographs were taken on an Eclipse TS100 microscope (Nikon) with a 10/0.25 (air) objective (Nikon), and a digital sight camera (Nikon). Two random fields per well were taken, and cells were counted with ImageJ (imagej.nih.gov/ij/; NIH). The number of invaded cells was normalized to the control with MDA-MB-231 cells with FBS gradient. Statistical evaluation with the *t* test.

Chemotaxis Assay. In a ClearView 96-well cell migration plate (Essen BioScience) 1,000 MDA-MB-231 cells per well were seeded into DMEM with 2.5% FBS after coating with fibronectin. Different concentrations of EGF (cell signaling) as chemoattractant were added to the assay medium (DMEM with 2.5% FBS) in the bottom chamber. On an IncuCyte S3 (Sartorius), the migration of cells to the bottom well was monitored over 72 h and afterward integrated into the area under the curve (AUC). Migration of control cells with no chemoattractant was subtracted from the signals. Mean ± SD of three wells for each point are given.

Live Cell Tracking. Real-time observation of cell migration was performed on μ-Slide 3D chemotaxis slides (ibidi). Preparation and implementation were carried out according to the manufacturer's instructions. 10,000 MDA-MB-231 derived cells were seeded into the center channel and allowed to adhere for 3 h. The two reservoirs contained RPMI medium with 0 and 10% FBS to generate an attractant gradient. Micrographs were taken every 10 min for 12 h under a microscope (Nikon eclipse Ti with Andor sCMOS camera) at 37 °C with 5% CO_2 atmosphere. The cells were tracked using ImageJ (imagej.nih.gov/ij/; NIH). The generation of trajectories and calculation of forward migration index (FMI) and velocities were performed using chemotaxis and migration tool software (ibidi). Statistical evaluation with the Mann–Whitney test (FMI) and *t* test (velocity).

Cell Proliferation Assay. MDA-MB-231 or indicated cell line derivatives thereof were seeded into a fibronectin-coated 96-well plate at 20,000 cells per well with RPMI and 1% FBS 24 h before labeling, fixating, and staining the cells with the Click-iT EdU Alexa Fluor 488 Kit (Thermo Fisher Scientific) according to the manufacturer's instructions. Micrographs were taken on a fluorescence microscope (Nikon Eclipse Ts2 with DS-Fi3 camera) with filters to visualize the total cell number (DAPI) and proliferating cells (FITC). EdU Alexa Fluor 488 incorporated cells were normalized to the total cell count. Statistical evaluation by the Mann–Whitney test.

Global Cell Adhesion Assay. MDA-MB-231 or indicated subcell lines thereof were stained with Calcein AM (Thermo Fisher Scientific) according to the instructions before seeding 20,000 cells per well into a fibronectin coated 96-well plate with RPMI and 10% FBS. After 30 min at 37 °C and 5% CO_2 unattached cells were washed away with PBS, and the calcein AM fluorescence was measured in a plate reader (Tecan). Data were normalized to a control where the unattached, normal MDA-MB-231 cells, were not washed away. Statistical evaluation by the Mann–Whitney test.

Lamellipodial Protrusions. MDA-MB-231 derived WAVE2 knockout cells with restored wt- or mt-WAVE2 were transduced lentivirally with Lifeact-iRFP670 to visualize filamentous Actin at the bottom of living cells using TIRF microscopy. pLenti Lifeact-iRFP670 BlastR was a gift from Ghassan Mouneimne (Addgene plasmid # 84385; http://n2t.net/addgene:84385; RRID:Addgene_84385). Cells were seeded into a starving medium (RPMI with 1% BSA, 0.05% FBS) in 8-well μ-slides (ibidi) coated with fibronectin (Roche). After 24 h, cells were stimulated with 500 ng/ml EGF (cell signaling) in RPMI and TIRF micrographs (Nikon eclipse Ti with Andor sCMOS camera) were taken every 5 s for 5 min directly after stimulation. Using ImageJ (imagej.nih.gov/ij/; NIH) the growing membrane protrusions of each cell were identified via F-actin stain. A random selection of protrusions was investigated by the generation of kymographs along a line orthogonal to the initial membrane as shown in *SI Appendix*, Fig. S6. Within the Kymograph, the transition from bright filamentous actin to the dark environment of the cell is defined as the leading edge (Fig. 3*A*, green curve). Faster-growing membrane bursts that are also characterized by fast retraction are visible as spike-like structures (Fig. 3*A*, pink curve). Protrusion of the leading edge, as well as the membrane bursts, occur simultaneously and at the same site. Membrane ruffles could be excluded as they occur dorsolateral and are not resolved in TIRF microscopy. Protrusion velocities were calculated. Statistical significance was evaluated using t test analysis for the leading edge and Mann–Whitney test for the bursts.

Actin Polymerization. The assay was performed in a quartz cuvette where pyrene fluorescence was measured at 25 °C on a spectrofluorometer (FP-6500 with temp.-controller ADP-303T, Jasco) using 2 mg/ml rabbit muscle actin with 25% pyrene-labeled actin (cytoskeleton) and the following proteins: 10 nM ARP2/3 (cytoskeleton), 15 μM PFN1, 12.5 nM VASP, and 25 nM PRM^{wt}-VCA or PRM^{GSPP}-VCA. Actin and the proteins were ultracentrifuged each at 4 °C and 100,000×*g* (Beckmann) for 45 min to reduce the number of aggregates. Two solutions were freshly prepared and combined to 1 × KMEI buffer directly before starting the measurement (40) where i) actin and pyrene-labeled actin with PFN1 in 5 mM Tris, 0.2 mM $CaCl_2$, pH 8.0 were mixed 10:1 with 10M1E buffer (10 mM EGTA, 1 mM $MgCl_2$, 1 mM Imidazole) and incubated for 1 min to exchanged calcium to magnesium and ii) remaining proteins in 10 × KMEI buffer (0.5 M KCl, 10 mM $MgCl_2$, 10 mM EGTA, 100 mM imidazole, and 10 mM TCEP, pH 7.0).

MDA-MB-231 Cell Extravasation in Embryonic Zebrafish Xenograft Model. The experiments with transgenic zebrafish embryos were conducted in a licensed establishment for the breeding and use of experimental animals [Leiden University (LU)] and subject to internal regulations and guidelines, stating that advice was taken from the Animal Welfare Body to minimize suffering for all experimental animals housed at the facility. The zebrafish assays described are not considered an animal experiment under the Experiments on Animals Act (Wod, effective 2014), the applicable legislation in the Netherlands in accordance with the European guidelines (EU directive no. 2010/63/EU) regarding the protection of animals used for scientific purposes. Therefore, a license specific for these assays on zebrafish larvae (<5 d) was not required.

Experiments were performed with transgenic zebrafish embryos (*fli*:EGFP), the vasculatures of which are marked in green, at 48 h postfertilization as described before (43). Zebrafish were maintained at 34 °C, a compromise for both the fish and the human cell lines.

For cancer cell extravasation approximately 400 of indicated cells were injected into the duct of curvier (DoC). Five days after the DoC injection, the number of cancer cells that extravasated individually from circulation into the collagen fibers of the tail fin was analyzed under a confocal microscopy (SP5 STED, Leica Microsystems). Statistical differences were determined by the t test.

In Vivo Mouse Cancer Cell Xenograft Studies. EPO Experimentelle Pharmakologie & Onkologie, Germany performed animal studies and AZ Biopharm, Germany analyzed blood plasma samples.

For pharmacokinetic investigations, osmotic pumps (1003D, Alzet) filled with 100 μl of EVH1 inhibitor were implanted subcutaneously into three female NMRI:nu/nu immunodeficient mice and blood plasma samples were taken at day three after implantation for inhibitor concentration determination. The applied dose corresponds to approximately 100 mg/kg twice a day. In comparison, three mice were treated directly with a dose of 100 mg/kg subcutaneously, and blood plasma samples were taken on 1, 6, and 24 h.

To compare WAVE2 knockout MDA-MB-231 cell lines restored with wt or mt WAVE2, a 1:1 mixture of Matrigel and 2.5 × 10^6 cells each was implanted orthotopically into the mammary fat pad of 7 female NOG mice per group. Over time, body weight was measured, and primary tumor size was calculated via caliper. The animals were investigated for macrometastasis after termination. Statistical differences were determined by t test analysis.

For studying the Ena/VASP-EVH1 inhibitor in the xenograft cancer model, 5 × 10^5 PANC-1 cells mixed 1:1 with Matrigel were implanted orthotopically into female NMRI:nu/nu mice. Animals with the subcutaneous (s.c.) application route were treated with a dose of 100 mg/kg twice a day starting one day after tumor inoculation. After 48 d the study was terminated, and the animals were investigated for macrometastasis. Statistical differences were determined by the Mann–Whitney test. Furthermore, the weights for tumors, liver, and lung were measured and compared using t test analysis. Termination criteria for all assays were defined as primary tumor volume greater than 1 cm^3 or, alternatively, behavioral changes due to tumor disease.

Statistics. Statistical analysis of the results was carried out with SigmaPlot 11. Three levels of statistical significance are distinguished and plotted in the text figures: $*P < 0.05$; $**P < 0.01$; $***P < 0.001$. Differences were considered significant at $P < 0.05$.

Data, Materials, and Software Availability. All study data are included in the article and/or *SI Appendix*.

ACKNOWLEDGMENTS. We thank Linda Ball for providing the GST-fused human VASP-EVH1 vector. This work is supported by the German Federal Ministry of Education and Research (16GW0186K), the European Innovation Council (190154511), ZonMW grant (09120012010061), and the collaboration project ProMTAC (TKI-LSH-DT2023-LUMC: 2024-02) that is cofunded by the PPP allowance made available by Health~Holland, Top Sector Life Sciences & Health, to stimulate public–private partnerships.

Author affiliations: [a]PROSION Therapeutics, Köln 50931, Germany; [b]Leibniz-Forschungsinstitut für Molekulare Pharmakologie, Berlin 13125, Germany; [c]Translational Immunology, Berlin Institute of Health at Charité-Universitätsmedizin Berlin, Berlin 10117, Germany; [d]Oncode Institute, Department of Cell and Chemical Biology, Leiden University Medical Center, Leiden 2333, The Netherlands; and [e]Department of Chemistry, University of Cologne, Köln 50939, Germany

1. J. E. Talmadge, I. J. Fidler, AACR centennial series: The biology of cancer metastasis: Historical perspective. *Cancer Res.* **70**, 5649–5669 (2010).
2. S. Maheswaran, D. A. Haber, Circulating tumor cells: A window into cancer biology and metastasis. *Curr Opin Genet Dev* **20**, 96–99 (2010).
3. J. Fares, M. Y. Fares, H. H. Khachfe, H. A. Salhab, Y. Fares, Molecular principles of metastasis: A hallmark of cancer revisited. *Signal Transduct. Target Ther.* **5**, 28 (2020).
4. D. Kedrin, J. van Rheenen, L. Hernandez, J. Condeelis, J. Segall, Cell motility and cytoskeletal regulation in invasion and metastasis. *J. Mammary Gland Biol. Neoplasia* **12**, 143–52 (2007).
5. G. P. Coló, E. M. Lafuente, J. Teixidó, The MRL proteins: Adapting cell adhesion, migration and growth. *Eur. J. Cell Biol.* **91**, 861–868 (2012).
6. J. A. Legg, L. M. Machesky, MRL proteins: Leading Ena/VASP to Ras GTPases. *Nat. Cell Biol.* **6**, 1015–1017 (2004).
7. S. Kurisu, T. Takenawa, The WASP and WAVE family proteins. *Genome Biol.* **10**, 226 (2009).
8. B. Chen *et al.*, The WAVE regulatory complex links diverse receptors to the actin cytoskeleton. *Cell* **156**, 195–207 (2014).
9. C. F. Stovold, T. H. Millard, L. M. Machesky, Inclusion of Scar/WAVE3 in a similar complex to Scar/WAVE1 and 2. *BMC Cell Biol.* **6**, 11 (2005).
10. H. Miki, H. Yamaguchi, S. Suetsugu, T. Takenawa, IRSp53 is an essential intermediate between Rac and WAVE in the regulation of membrane ruffling. *Nature* **408**, 732–735 (2000).
11. A. M. Ismail, S. B. Padrick, B. Chen, J. Umetani, M. K. Rosen, The wave regulatory complex is inhibited. *Nat. Struct. Mol. Biol.* **16**, 561–563 (2009).
12. Z. Chen *et al.*, Structure and control of the actin regulatory WAVE complex. *Nature* **468**, 533–538 (2010).
13. A.-L. Law *et al.*, Lamellipodin and the Scar/WAVE complex cooperate to promote cell migration in vivo. *J. Cell Biol.* **203**, 673–689 (2013).
14. G. Carmona *et al.*, Lamellipodin promotes invasive 3D cancer cell migration via regulated interactions with Ena/VASP and SCAR/WAVE. *Oncogene* **35**, 5155–5169 (2016).
15. M. Krause, E. W. Dent, J. E. Bear, J. J. Loureiro, F. B. Gertler, Ena/VASP proteins: Regulators of the actin cytoskeleton and cell migration. *Annu. Rev. Cell Dev. Biol.* **19**, 541–564 (2003).
16. D. Breitsprecher *et al.*, Clustering of VASP actively drives processive, WH2 domain-mediated actin filament elongation. *EMBO J.* **27**, 2943–2954 (2008).
17. S. D. Hansen, R. D. Mullins, Lamellipodin promotes actin assembly by clustering Ena/VASP proteins and tethering them to actin filaments *eLife* **4**, e06585 (2015), 10.7554/eLife.06585
18. M. C. Mendoza *et al.*, Erk-MAPK drives lamellipodia protrusion by activating the WAVE2 regulatory complex. *Mol. Cell* **41**, 661–671 (2011).
19. C. Bachmann, L. Fischer, U. Walter, M. Reinhard, The EVH2 domain of the vasodilator-stimulated phosphoprotein mediates tetramerization, F-actin binding, and actin bundle formation. *J. Biol. Chem.* **274**, 23549–23557 (1999).
20. J. E. Bear *et al.*, Antagonism between Ena/VASP proteins and actin filament capping regulates fibroblast motility. *Cell* **109**, 509–521 (2002).
21. L. J. Ball, T. Jarchau, H. Oschkinat, U. Walter, EVH1 domains: Structure, function and interactions. *FEBS Lett.* **513**, 45–52 (2002).
22. J. E. Bear *et al.*, Negative regulation of fibroblast motility by Ena/VASP proteins. *Cell* **101**, 717–728 (2000).
23. M. Krause *et al.*, Lamellipodin, an Ena/VASP ligand, is implicated in the regulation of lamellipodial dynamics. *Dev. Cell* **7**, 571–583 (2004).
24. U. Philippar *et al.*, A mena invasion isoform potentiates EGF-induced carcinoma cell invasion and metastasis. *Dev. Cell* **15**, 813–828 (2008).
25. W. Wang *et al.*, Identification and testing of a gene expression signature of invasive carcinoma cells within primary mammary tumors. *Cancer Res.* **64**, 8585–8594 (2004).
26. D. Chen *et al.*, Enah overexpression is correlated with poor survival and aggressive phenotype in gastric cancer. *Cell Death Dis.* **9**, 998 (2018).
27. L.-D. Hu, H.-F. Zou, S.-X. Zhan, K.-M. Cao, EVL (Ena/VASP-like) expression is up-regulated in human breast cancer and its relative expression level is correlated with clinical stages. *Oncol. Rep.* **19**, 1015–1020 (2008).
28. U. Philippar *et al.*, Ena/VASP proteins promote cancer cell invasion. *Cancer Res.* **67**, 559A (2007).
29. X. Xiang *et al.*, Vasodilator-stimulated phosphoprotein promotes liver metastasis of gastrointestinal cancer by activating a β1-integrin-FAK-YAP1/TAZ signaling pathway. *NPJ Precis. Oncol.* **2**, 2 (2018).
30. J. Zaminer *et al.*, Addressing protein–protein interactions with small molecules: A pro-pro dipeptide mimic with a PPII helix conformation as a module for the synthesis of PRD-binding ligands. *Angew. Chem. Int. Ed. Engl.* **49**, 7111–7115 (2010).
31. C. Reuter, P. Huy, J.-M. Neudörfl, R. Kühne, H.-G. Schmalz, Exercises in pyrrolidine chemistry: Gram scale synthesis of a Pro-Pro dipeptide mimetic with a polyproline type II helix conformation. *Chem. Eur. J.* **17**, 12037–12044 (2011).
32. V. Hack *et al.*, Efficient α-helix induction in a linear peptide chain by N-capping with a bridged-tricyclic diproline analogue. *Angew. Chem. Int. Ed. Engl.* **52**, 9539–9543 (2013).
33. C. Reuter *et al.*, Stereoselective synthesis of proline-derived dipeptide scaffolds (ProM-3 and ProM-7) rigidified in a PPII helix conformation. *Eur. J. Org. Chem.* **2014**, 2664–2667 (2014).
34. C. Reuter *et al.*, Design and stereoselective synthesis of ProM-2: A spirocyclic diproline mimetic with polyproline type II (PPII) helix conformation. *Chem. Eur. J.* **21**, 8464–8470 (2015).
35. S. Chiha *et al.*, Design and synthesis of building blocks for PPII-helix secondary-structure mimetics: A stereoselective entry to 4-substituted 5-vinylprolines. *Eur. J. Organic Chem.* **2018**, 6597–6597 (2018).
36. S. Dohmen *et al.*, Pd-catalyzed asymmetric n-allylation of amino acid esters with exceptional levels of catalyst control: Stereo-divergent synthesis of ProM-15 and related bicyclic dipeptide mimetics. *Chem. Eur. J.* **26**, 3049–3053 (2020).
37. R. Opitz *et al.*, A modular toolkit to inhibit proline-rich motif–mediated protein–protein interactions. *Proc. Natl. Acad. Sci. U.S.A.* **112**, 5011–5016 (2015).
38. M. Barone *et al.*, Designed nanomolar small-molecule inhibitors of Ena/VASP EVH1 interaction impair invasion and extravasation of breast cancer cells. *Proc. Natl. Acad. Sci. U.S.A.* **117**, 29684–29690 (2020).
39. L. A. Acevedo, A. I. Greenwood, L. K. Nicholson, A noncanonical binding site in the EVH1 domain of vasodilator-stimulated phosphoprotein regulates its interactions with the proline rich region of zyxin. *Biochemistry* **56**, 4626–4636 (2017).
40. X. J. Chen *et al.*, Ena/VASP proteins cooperate with the WAVE complex to regulate the actin cytoskeleton. *Dev. Cell* **30**, 569–584 (2014).
41. S. Havrylenko *et al.*, Wave binds Ena/VASP for enhanced Arp2/3 complex–based actin assembly. *Mol. Biol. Cell* **26**, 55–65 (2015).
42. C. Litschko *et al.*, Differential functions of WAVE regulatory complex subunits in the regulation of actin-driven processes. *Eur. J. Cell Biol.* **96**, 715–727 (2017).
43. J. Ren, S. Liu, C. Cui, P. Dijke, Invasive behavior of human breast cancer cells in embryonic zebrafish. *J. Vis. Exp.* **122**, 55459 (2017).
44. Y. Drabsch, B. E. Snaar-Jagalska, P. Ten Dijke, Fish tales: The use of zebrafish xenograft human cancer cell models. *Histol. Histopathol.* **32**, 673–686 (2017).
45. M. F. B. Nielsen, M. B. Mortensen, S. Detlefsen, Key players in pancreatic cancer-stroma interaction: Cancer-associated fibroblasts, endothelial and inflammatory cells. *World J. Gastroenterol.* **22**, 2678–2700 (2016).
46. R. F. Hwang *et al.*, Cancer-associated stromal fibroblasts promote pancreatic tumor progression. *Cancer Res.* **68**, 918–926 (2008).
47. M. Uhlén *et al.*, Proteomics. Tissue-based map of the human proteome. *Science* **347**, 1260419 (2015).
48. M. Michael, A. Vehlow, C. Navarro, M. Krause, c-Abl, Lamellipodin, and Ena/VASP proteins cooperate in dorsal ruffling of fibroblasts and axonal morphogenesis. *Curr. Biol.* **20**, 783–791 (2010).
49. F. Ferron, G. Rebowski, S. H. Lee, R. Dominguez, Structural basis for the recruitment of profilin-actin complexes during filament elongation by Ena/VASP. *EMBO J.* **26**, 4597–4606 (2007).
50. S. D. Hansen, R. D. Mullins, VASP is a processive actin polymerase that requires monomeric actin for barbed end association. *J. Cell Biol.* **191**, 571–584 (2010).
51. L. J. Ball *et al.*, Dual epitope recognition by the VASP EVH1 domain modulates polyproline ligand specificity and binding affinity. *EMBO J.* **19**, 4903–4914 (2000).
52. F. A. Ran *et al.*, Genome engineering using the CRISPR-Cas9 system. *Nat. Protoc.* **8**, 2281–2308 (2013).
53. Regulators and Effectors of Small GTPases: Rho Family, Volume 406–1st Edition|Elsevier Shop. https://shop.elsevier.com/books/regulators-and-effectors-of-small-gtpases-rho-family/balch/978-0-12-182811-0.
54. S. Lange, M. Sylvester, M. Schümann, C. Freund, E. Krause, Identification of phosphorylation-dependent interaction partners of the adapter protein ADAP using quantitative mass spectrometry: SILAC vs 18O-labeling. *J. Proteome Res.* **9**, 4113–4122 (2010).
55. H. N. Heine, *Peptidmimetika an Zellulosemembranen* (Humboldt-Universität zu Berlin, Mathematisch-Naturwissenschaftliche Fakultät I, 2000). 10.18452/14537.